Compaction behavior of powder bed fusion feedstock for metal and polymer additive manufacturing

Francesco Sillani
Inspire AG, St. Gallen, Switzerland and Institut für Werkzeugmaschinen und Fertigung, ETH Zurich, Zurich, Switzerland
Dominik Wagner
Institut für Werkzeugmaschinen und Fertigung, ETH Zurich, Zurich, Switzerland
Marvin Aaron Spurek and Lukas Haferkamp
Inspire AG, St. Gallen, Switzerland and Institut für Werkzeugmaschinen und Fertigung, ETH Zurich, Zurich, Switzerland
Adriaan Bernardus Spierings and Manfred Schmid
Inspire AG, St. Gallen, Switzerland, and
Konrad Wegener
Institut für Werkzeugmaschinen und Fertigung, ETH Zurich, Zurich, Switzerland

Abstract

Purpose – Powder bed-based additive manufacturing (AM) is a promising family of technologies for industrial applications. The purpose of this study is to provide a new metrics based on the analysis of the compaction behavior for the evaluation of flowability of AM powders.

Design/methodology/approach – In this work, a novel qualification methodology based on a camera mounted onto a commercially available tap density meter allowed to assess the compaction behavior of a selection of AM materials, both polymers and metals. This methodology automatizes the reading of the powder height and obtains more information compared to ASTM B527. A novel property is introduced, the "tapping modulus," which describes the packing speed of a powdered material and is related to a compression/vibration powder flow.

Findings – The compaction behavior was successfully correlated with the dynamic angle of repose for polymers, but interestingly not for metals, shedding more light to the different flow behavior of these materials.

Research limitations/implications – Because of the chosen materials, the results may lack generalizability. For example, the application of this methodology outside of AM would be interesting.

Originality/value – This paper suggests a new methodology for assessing the flowing behavior of AM materials when subjected to compression. The device is inexpensive and easy to implement in a quality assurance environment, being thus interesting for industrial applications.

Keywords Selective laser sintering, Flowability, Compaction, Powder bed fusion PBF, Selective laser melting SLM, Tap density

Paper type Research paper

1. Introduction

Additive manufacturing (AM) is attracting strong interest in many industries: production of end-use parts can be achieved within a few hours or days for an increasing number of applications.

Powder bed fusion (PBF) of both polymers and metals is the family of AM technologies that is closest to industrial applications: complex parts with a wide range of properties can be produced on demand and with much more design freedom compared to traditional machining. Nevertheless, the material range is still limited, and especially for selective laser sintering (PBF-LB/P, powder bed fusion of polymers with a laser beam, according to ISO/ASTM 52900 [ASTM International and ISO, 2018]), the material palette is mostly restricted to polyamide 12 (PA12) and its composites.

Recently, the interest of material suppliers to offer new polymer classes and metal alloys has grown. This is due to an overall PBF market growth, mainly driven by industrialization of this family of technologies, which can be estimated by

The current issue and full text archive of this journal is available on Emerald Insight at: **https://www.emerald.com/insight/1355-2546.htm**

Rapid Prototyping Journal
27/11 (2021) 58–66
Emerald Publishing Limited [ISSN 1355-2546]
[DOI 10.1108/RPJ-01-2021-0010]

Received 8 January 2021
Revised 26 March 2021
29 April 2021
18 May 2021
Accepted 28 May 2021

looking at the year-over-year growth of polymer and metal feedstock, which in 2018 was 37.9% and 41.9%, respectively (Caffrey and Wohler, 2019). Gas atomization and plasma rotating electrode processes have become the industrial standard for the production of metal powders for selective laser melting (PBF-LB/M, powder bed fusion of metals with a laser beam, according to ISO/ASTM 52900 [ASTM International and ISO, 2018]) and yield spherical powders with low amount of porosity, as reported by Sames *et al.* (2016). Polymer powders are currently produced through different routes: cryogenic milling is the most common technique for short time-to-market products, thanks to its simplicity compared to more complex processes such as dissolution–precipitation. The dissolution–precipitation procedure is carried out with ethanol as solvent in specific temperature and pressure conditions, as reported by Baumann and Wilczok (1998), and is used to produce PA12 particles characterized by a "potato" shape (Schmid *et al.*, 2017). Melt emulsification is used to produce powders from an immiscible mixture of a "carrier" and "target" polymer. The mixture is coextruded at high temperature, and then the "carrier" polymer is selectively washed away using an appropriate solvent that does not dissolve the "target" polymer. Vetterli (2019) reported a regular distribution of spherical particles for polypropylene produced through melt emulsification, and Kleijnen *et al.* (2019) confirmed the same for polybutylene terephthalate. Schmid *et al.* (2014) report that optimization of powder shape and size distributions brings significant advantages for flowability, for which the following definition from Gotoh *et al.* (2001) can be used: "[flowability represents the powder] ease of flow and relates to the change of mutual position of individual particles forming the powder bed." Gotoh also suggests numerous ways to assess flowability, as real powder flow typically occurs as a combination of different "flow patterns," a term that comes from fluid mechanics and that is used to define how a fluid flows through a reactor. Vock *et al.* (2019) report that the main flow pattern is strongly application dependent, whereas different expressions of flowability can refer to the same flow pattern. In AM, for example, the typical flowability metrics are angle of repose (gravitational, compression and fluidized flow) and compressibility (compression and vibration flow) (Vock *et al.*, 2019), both qualitatively depicted in Figure 1.

For polymers, the flowability measured through the angle of repose is critical for obtaining smooth powder layers and, consequently, an error-free processing (Amado, 2016). Vetterli (2019) reported a positive correlation between the final part density and the powder bed density, highlighting the importance of compressibility in PBM of polymers. Regarding metals, powder flowability (Spierings *et al.*, 2016; Seyda, 2018) and powder bed density (Spierings *et al.*, 2016; Li *et al.*, 2010; Ali *et al.*, 2018) are also often stressed as relevant influences on part density. Haferkamp *et al.* (2021), however, recently showed only a limited correlation between powder layer density (similar to powder bed density) and part density: this might mean that flowability affects PBM of polymers and metals in a different way.

Numerous examples in AM literature (Vetterli, 2019; Vock *et al.*, 2019; Amado, 2016; Ziegelmeier *et al.*, 2013; Berretta, 2015) suggest that the dynamic angle of repose, also called avalanche angle, is the most used mean to model the flowing

Figure 1 Different types of flowability expressions

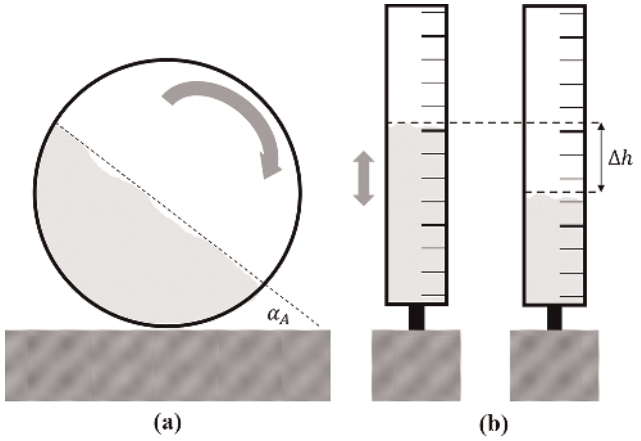

Notes: (a) Angle of repose as avalanche angle αA;
(b) compaction behavior as height difference Δh between loose and compacted powder

behavior during the recoating step. Kiani *et al.* (2020) and Spierings *et al.* (2016) furthermore argue that the avalanche angle measurement corresponds well to the process condition in PBF. The compaction behavior, on the other hand, is typically measured by the Hausner ratio H:

$$H = \frac{\rho_{tap}}{\rho_{bulk}} \tag{1}$$

where ρ_{bulk} and ρ_{tap} are defined as bulk and tap density, respectively, which are typically measured according to ASTM B417 (ASTM International, 2018) and ASTM B527 (ASTM International, 2015) standards.

ASTM B527, in particular, prescribes to let the powder compact inside of a cylinder with a certain diameter (depending on its material density ρ_m), subjected to an oscillating motion in the vertical direction with an amplitude of 3 mm for 3,000 periods (taps), as shown in Figure 2.

The final value of the powder volume V_{powder} is manually read from the cylinder and used to compute ρ_{tap} according to:

Figure 2 Schematic representation of ASTM B527 test execution

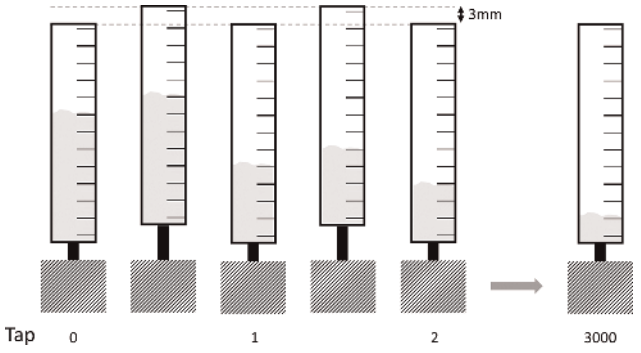

$$\rho_{tap} = \frac{m_{filled}}{V_{powder}} \quad (2)$$

where m_{filled} is the mass of powder inside of the cylinder and V_{powder} the value read by the operator at the end of compaction.

The tap density is the packing density of a powder in the highest possible state of compaction. When measuring the tap density according to ASTM B527, some information is lost, as powders can have the same Hausner ratio H but different curves when compacting from bulk to tap density. This has been already observed by Vetterli (2019), who compared two commercially available polyamide 12 powders: Duraform PA12 (3 D Systems, USA), produced using dissolution–precipitation (Baumann and Wilczok, 1998), and Orgasol Invent Smooth (Arkema, France), produced via direct solvent polymerization (Schmid *et al.*, 2017). The powders had a similar particle size but, because of their production process, different shape distributions. The device used by Vetterli (2019) was capable of recording the powder height after every tap, but the prescription of "compression under its own weight" reported in ASTM B527 was not respected because a metal disk was placed on the top powder surface. The obtained results showed very similar Hausner ratios but substantially different "compaction curves," as reported in Figure 3.

Scope of the current work is thus to investigate the compaction behavior of a selection of commercially available AM powders, both polymers and metals. The evaluation of the compaction behavior will be carried out with a novel approach on a device specifically designed for this purpose. Repeatability of the aforementioned device is validated, and it will provide additional insights on powder flowability under compression flow compared to the methodologies currently available on the market. Finally, the compaction behavior will be correlated with dynamic angle of repose α_A and Hausner ratio H to understand its possible utility as quality assurance method for PBF AM.

Figure 3 Compaction of Duraform PA12 (H = 1.13) and Orgasol Invent Smooth PA12 (H = 1.12) from Vetterli (2019)

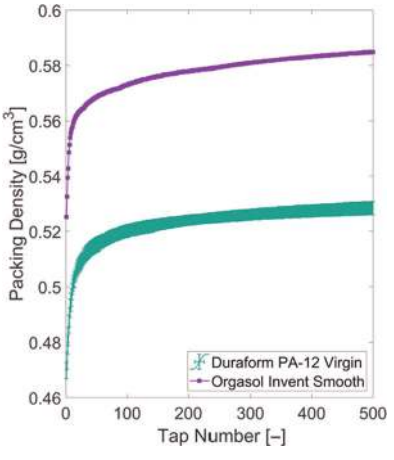

2. Materials and methods

2.1 Powders

This study was carried out on commercially available materials that cover a broad spectrum of size and shape distributions, as highlighted in subsection 3.1. All materials were tested as received, with no specific conditioning, and their data are reported in Table 1 and Table 2.

2.2 Particle size and shape distributions

The particle size distribution (PSD) was assessed using a LS230 laser diffraction device (Beckman Coulter – Brea, CA, USA) with conventional measurements taken on dispersed samples (0.03Wt.% in ethanol). A DM-6 (Leica – Wetzlar, Germany) optical microscope was used with the procedure introduced in the study of Sillani *et al.* (2019) to calculate the particle shape distribution. The shape was characterized using elliptic smoothness E_S after fitting each particle with an ellipse of same area, orientation and centroid as in Figure 4 using the software ImageJ.

The shape factor E_S was then calculated as follows:

$$E_S = \frac{P_{pa}}{P_{el}} \quad (3)$$

with P_{pa} being the perimeter of the particle and P_{el} the one of the fitted ellipse. The perimeter of the ellipse is calculated with:

$$P_{ellipse} = \pi \cdot (a+b) \cdot \left(1 + \frac{3h}{10 + \sqrt{4-3h}}\right) \quad (4)$$

according to Ramanujan (1914), where a and b are the major and minor axes of the ellipse, and $h = \left(\frac{a-b}{a+b}\right)^2$.

Using elliptic smoothness for metal feedstock is unusual, as the atomization process typically produces very spherical particles. Nevertheless, being circles a particular case of ellipses, and considering that in this work both polymer and metal feedstock are simultaneously analyzed, the usage of E_S seems reasonable in this context.

2.3 Evaluation of compaction behavior

A BeDensi T3 Tap Density Meter (Bettersize, Dandong, Liaoning, China) was modified and used for the measurement

Table 1 Polymer feedstock

Producer	Commercial name (short)	Material type	Production method
3 D Systems (Rock Hill, SC, USA)	Duraform PA12 (PA12-SLS)	Polyamide 12	Dissolution precipitation
EOS (Kreilling, Germany)	PA1102 (PA11-SLS)	Polyamide 11	Cryogenic grinding + particle rounding
Diamond Plastics (Gräfenberg, Germany)	Laser PP CP 50 (PP-SLS-1)	Polypropylene	Cryogenic grinding
Aspect (Tokyo, Japan)	iCoPP (PP-SLS-2)	Polypropylene	Melt emulsification
3 D Systems (Rock Hill, SC, USA)	Duraform Flex (TPE-SLS)	Thermoplastic elastomer	Cryogenic grinding

Table 2 Metal feedstock

Producer	Commercial name (short)	Material type	Production method
Carpenter (Philadelphia, PA, USA)	Micro Melt 316 L 15 μm (316 L-MIM-1)	1.4404 stainless steel	Gas atomization
CNPC (Shanghai, China)	SS316 powder D50 30 μm to 50 μm (316 L-SLM)	1.4404 stainless steel	Gas atomization
Praxair (Danbury, CT, USA)	FE 271–1 (316 L-MIM-2)	1.4404 stainless steel	Gas atomization
IMR Metal powder technologies GmbH (Velden am Wörthersee, Austria)	AlSi10Mg Gries (A360-SLM-1)	AlSiMg10	Gas atomization
Tekna Advanced Materials Inc. (Sherbrooke, QC, Canada)	AlSi10Mg-64/20-CS05 (A360-SLM-2)	AlSiMg10	Plasma atomization

Figure 4 Ellipse fitting

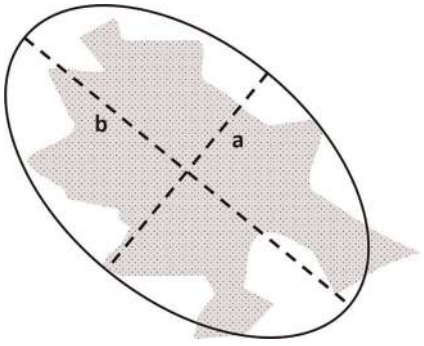

Figure 5 Modified tap density meter

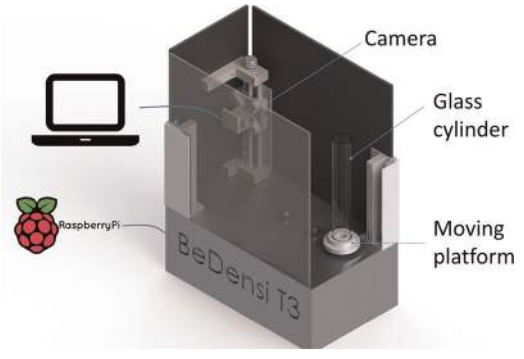

of the compaction behavior. The existing motor controller of the device was replaced with a Raspberry Pi 3 Model B+ (Raspberry Pi Foundation, Cambridge, UK) and a IDS UI-3360CP (IDS Imaging Development Systems GmbH, Obersulm, Germany) camera for the automated evaluation of the powder height was integrated. The final setup is depicted in Figure 5.

The bulk density ρ_{bulk} of each powder was assessed according to ASTM B417, and then the weight of 90 cm^3 of material was calculated with:

$$m_{powder} = 90\ \text{cm}^3 \cdot \rho_{bulk} \tag{5}$$

Afterwards, this amount of powder was weighted using a AE200 balance with a AB33360 measuring unit (Mettler Toledo, Schwerzenbach, Switzerland) and carefully inserted into the glass cylinder using a funnel. The measurement itself consisted of 1,000 taps at two different tapping frequencies with 3 mm motion amplitude, whereas a video was being recorded using the camera. The first frequency was selected to be 0.16 Hz for taps 1 to 25, whereas the second tapping frequency used was 2 Hz for taps 26 to 1,000. Compared to the recommended values of 1.6 Hz to 5 Hz (ASTM B527), these tapping frequencies were selected to allow complete powder movement after each tap (settling). A MATLAB [textregistered] script was first used to calculate the height of the powder $h(t_x)$ for every frame x, as shown in Figure 6.

Afterwards, each tap was automatically recognized, as highlighted in Figure 7.

The same script automatically calculated the settling volume V_i^{set} from the evaluation of $h(t_x)$ between 70% and 90% of the time t_{i+1}, when the powder is assumed to be settled. The subscripts i and x in Figure 7 are counting the taps and video frames, respectively.

Then, the settling volume V_i^{set} of every tap i was converted into powder density ρ_i according to:

$$\rho_i = \frac{90\ \text{cm}^3}{V_i^{set}} \cdot \rho_{bulk} \tag{6}$$

Following relations also hold:

$$\lim_{i \to 0^+} \rho_i = \rho_{bulk} \tag{7}$$

$$\lim_{i \to 3000^-} \rho_i = \rho_{tap} \tag{8}$$

Figure 6 Image recognition process from raw data to $h(t_x)$

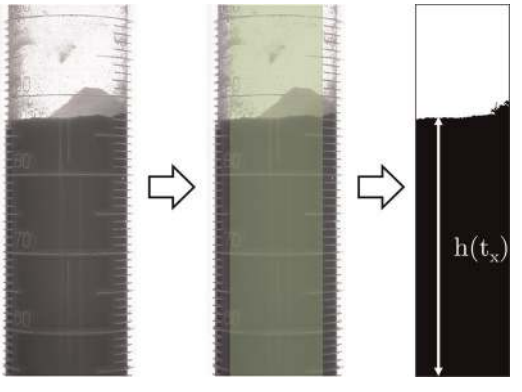

Figure 7 Sample output used for image analysis, reporting the powder height in pixel vs time in frames

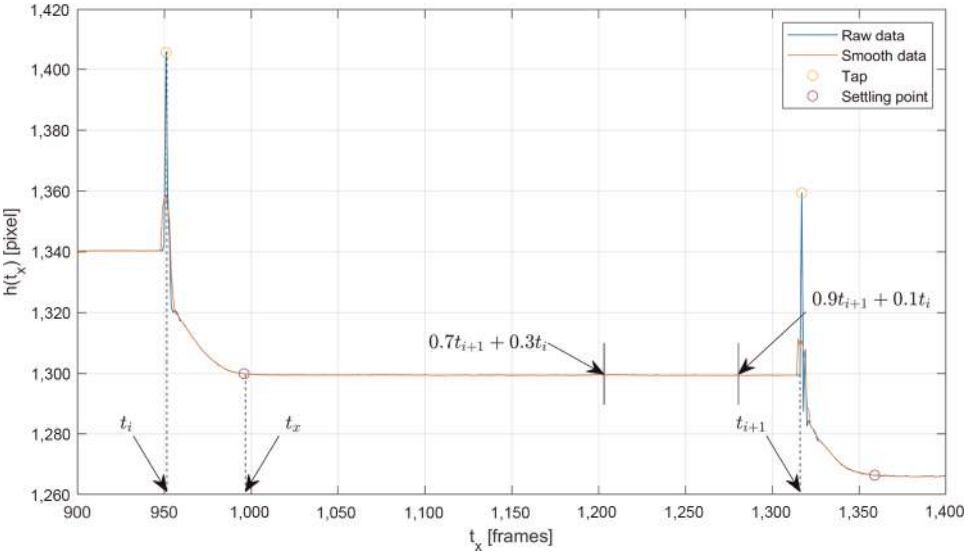

2.4 Evaluation of dynamic angle of repose

A REVOLUTION Powder Analyzer (Mercury Scientific – Newton, CT, USA) was used to assess the dynamic angle of repose α_A. The measurement was repeated three times for every sample, with 128 avalanches recorded per run. The dynamic angle of repose was calculated for every avalanche, and an average value was used.

2.5 Characterization of compaction curve

Each compaction curve was first normalized for every tap i using as follows:

$$\tilde{\rho}_i = \frac{\rho_i - \min(\rho_i, \forall i)}{\max(\rho_i, \forall i) - \min(\rho_i, \forall i)} \cdot 100 \tag{9}$$

where ρ_i is the absolute density calculated at the tap , and $\tilde{\rho}_i$ is the density at tap i, normalized between 0% and 100% according to the minimum and maximum values of ρ_i.

Then, a linear regression was applied to the first 15 data points to capture the most linear part of the compaction behavior. The slope of the obtained line is defined as the normalized tapping modulus $\tilde{T_{15}}$ and describes the packing velocity of the powder in absolute units. This way, materials with different ρ_m can be compared.

2.6 Repeatability evaluation of setup

The performances of modified tapping device introduced in this work had to be statistically evaluated to assess its repeatability. Every material was tested five times by the same operator, and the variance per feedstock was then calculated according to the procedure outlined in Figure 8.

All the five curves referring to the same powder are used to obtain an average powder density after every tap $\overline{\rho_i}$ and its standard deviation $SD_{\rho,i}$, as shown in Figure 8(a). To compare the repeatability of the measurement procedure for powders characterized by different ρ_m, the relative standard deviation of the powder density is also calculated according to:

Figure 8 Repeatability evaluation outline

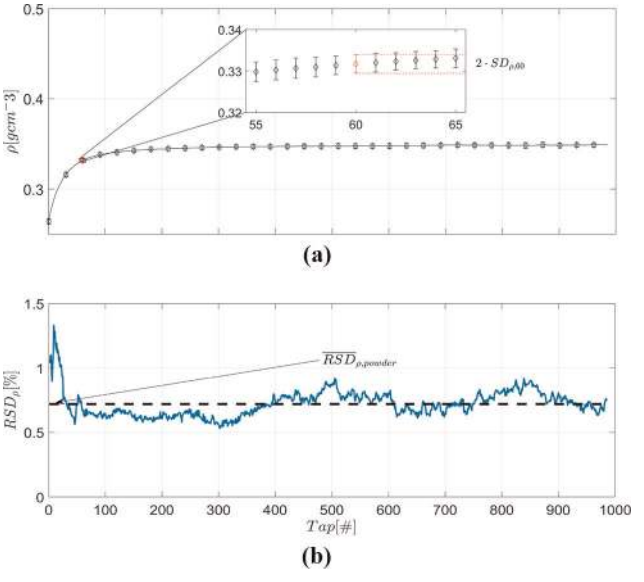

Notes: (a) Average compaction curve with standard deviation for every tap; (b) relative standard deviation for every tap

$$\overline{RSD}_{\rho,powder} = \frac{1}{1000} \sum_{i=1}^{1000} \frac{SD_{\rho,i}}{\overline{\rho_i}} \cdot 100 \tag{10}$$

as shown in Figure 8(b) with the black dashed line.

3. Results and discussion

3.1 Material selection

The feedstock used for this work was chosen to cover a variety of powder properties and to show the suitability of the proposed methodology to study the flowability of AM materials. The

powder data set comprises size distribution [Figure 9(a)], shape distribution (Figure 9(c)] and flowability [Figure 9(b), Hausner ratio H and Figure 9(d), avalanche angle α_A]. The verification was done qualitatively by plotting the most relevant properties of each powder: this analysis shows that the chosen materials are covering a wide spectrum of characteristics, and this supports a wide applicability of the proposed methodology for the evaluation of compression/vibration flow for AM feedstock.

3.2 Compaction behavior – Tapping modulus

Compaction curves for all the powders were measured following the procedure in subsection 2.3, and the average curve for each material is shown in Figure 10(a). To assess the compression/vibration flow behavior associated with each material, all curves were further characterized according to the methodology in subsection 2.5. The results of the linear regression are reported in Figure 10(b) together with the quality of the fit R^2, whereas $\tilde{T_{15}}$ is reported in Table 3.

Materials exhibiting higher $\tilde{T_{15}}$ values are compacting faster and, therefore, are characterized by a better flowability. In this sense, PP-SLS-2 and 316 L-MIM-2 show the best flowability in the two material classes. It is noteworthy to observe that 316 L-MIM-1 and 316 L-MIM-2 exhibit a different value of $\tilde{T_{15}}$, but are clearly characterized by a very similar size, shape and flowability (avalanche angle and Hausner ratio). 316 L-MIM-1 is characterized by a bit smaller PSD, and in this size range, this is probably enough to justify a major difference in flowability, at least the one measured with the proposed methodology, which seems to have a good sensitivity toward fine differences in the powder morphology.

To better understand the utility of the $\tilde{T_{15}}$ in the characterization of AM materials, a comparison with the shape factor E_S, the median diameter D_{50V} and the avalanche angle α_A is reported in Figure 11 for polymers (left) and metals (right). By looking at the Pearson's correlation coefficient r, reported on the bottom left of each graph shown in Figure 11 in red when statistically significant, it is clear that the two material classes are affected differently by size and shape distributions. The size of metal powder (here represented by D_{50V}) is inversely proportional to tapping modulus $\tilde{T_{15}}$, with $r = -0.95$. This means that coarser powders compact slower, possibly because of a lower void fraction after pouring the powder into the container. When comparing powders with similar density ρ_m (1 for polymers, 2.7 for aluminum, 7.8 for steel, all in g cm^{-3}) and different D_{50V} but similar shape ($E_S \approx 1$ for metals), gravitational forces can be assumed to scale with D_{50V}, and intuitively, this could be an explanation for the observed behavior. During the filling procedure, powders with a higher single-particle mass (due to higher D_{50V}) compact more, leading to a lower void fraction and thus exhibiting a lower tapping modulus. Also, during tapping, powders composed of particles with higher mass are more easily dragged down by gravity and thus compact faster. On the other hand, shape (here represented by E_S) seems determinant for polymers: with a $r = -0.88$, particles characterized by rougher edges (higher E_S) compact slower and to a lesser extent. Hence, size and shape distributions of the powder, which are determined by the production process, play a determinant role for flowability, and the data reported in Figure 11(b) is confirming that melt

Figure 9 Feedstock property space

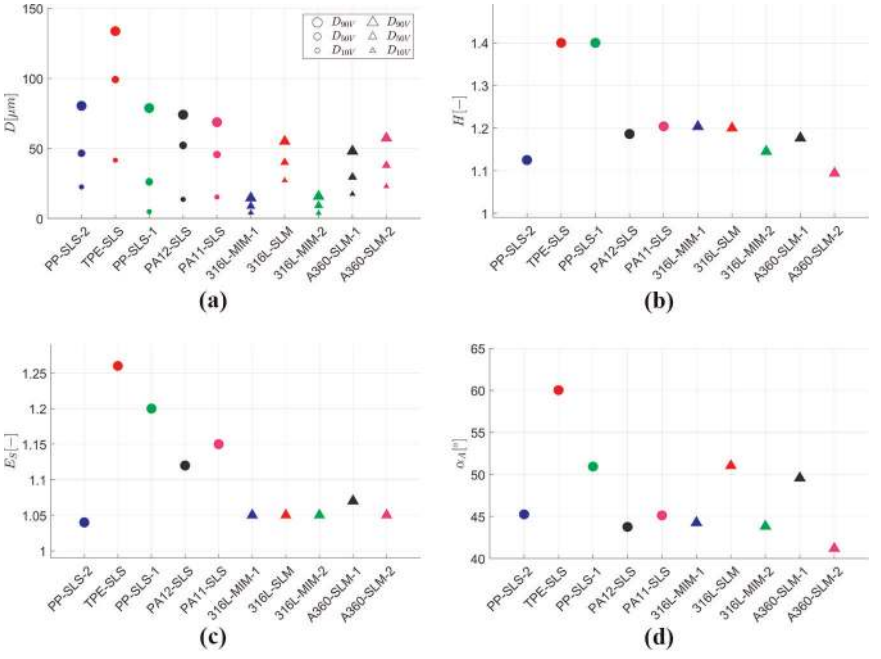

Notes: (a) Diameter; (b) hausner ratio; c) elliptic smoothness; (d) avalanche angle

Figure 10 Compaction behavior

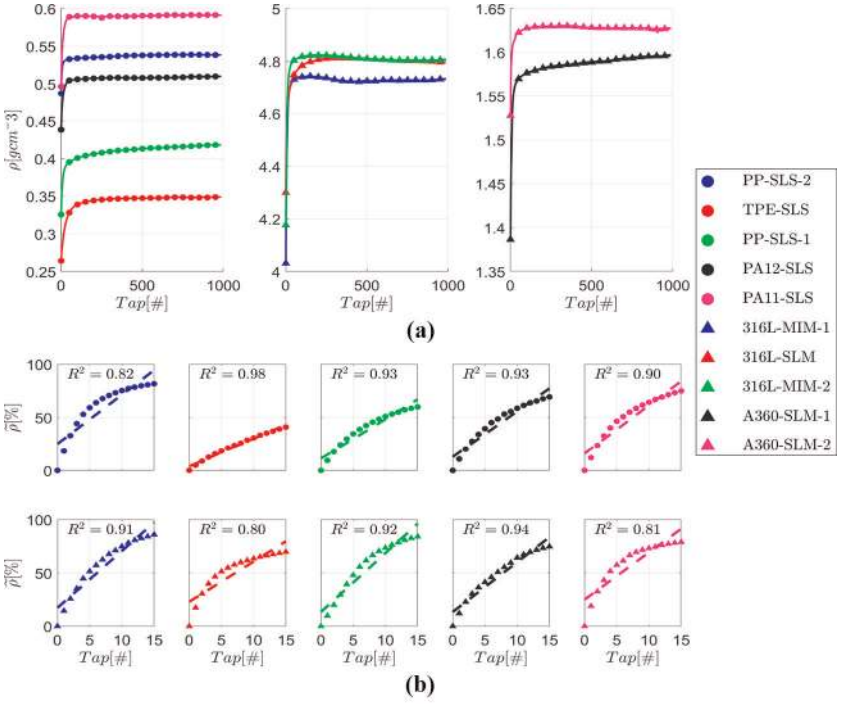

Notes: (a) Average compaction curves for all feedstock; (b) normalized tapping modulus

Figure 11 Flowability comparison with powder properties, divided for polymers (left) and metals (right)

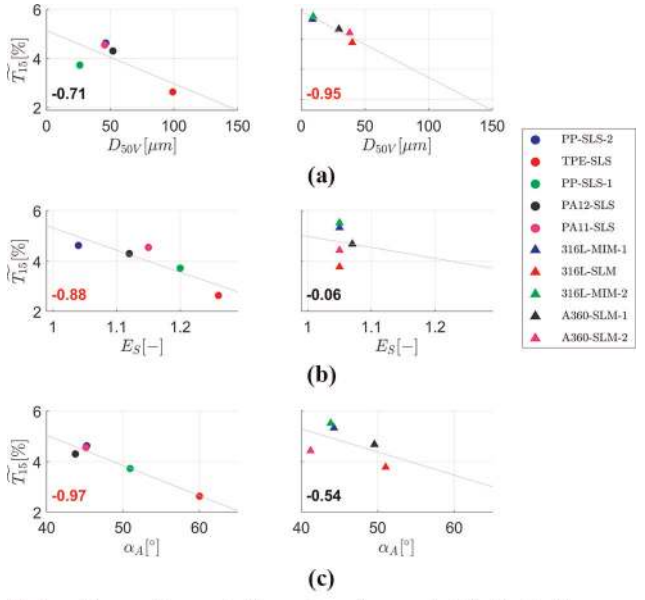

Notes: Pearson's correlation value r is reported in the bottom left part of the graph in red when statistically significant; (a) normalized tapping modulus vs particle size; (b) normalized tapping modulus vs particle shape; (c) normalized tapping modulus vs avalanche angle

emulsification allows to obtain smooth and well-flowing materials (Kleijnen *et al.*, 2019). Rietema (1991) reports that cohesion forces, such as Van der Waals', scale inversely with the surface roughness of particles (intended as size and surface density of asperities) and directly with their hardness. Rietema qualitatively estimates the ratio of cohesive forces vs gravitational $\frac{F_c}{F_g}$ for powders characterized by particles with the same size and shape and finds an increase of cohesive forces as ρ_m decreases. Hence, the lack of statistically significant correlation between D_{50V} and $\tilde{T}_{15}$ for polymers holds also from the physical point of view, as gravitational forces are (relatively) less important than in metal samples, where the correlation is significant ($r = -0.95$). Also, as cohesive forces become more important for less dense materials, shape (at similar D_{50V}) also becomes more relevant for the (initial) packing behavior of polymers. When additional energy is added to the system, e.g. through vibration such as in the proposed experiment, other properties become probably more important, for example, particle-to-particle friction and interlocking (both increase with increasing E_S), as can be intuitively assumed. The flow pattern induced by the tapping setup is different from the one occurring in the rotating drum introduced in subsection 2.4: there, a fluidized flow occurs, and thus, results are expected to be substantially different. The avalanche angle α_A is directly related to the proposed normalized tapping modulus $\tilde{T}_{15}$ in Figure 11(c), and a significant correlation between the two flow patterns exists for polymer feedstock ($r = -0.97$). In contrast,

the compaction flow is different from the fluidized flow for metal samples, for which r is not significant.

3.3 Compaction behavior – Repeatability study

Compaction curves for all feedstock were shown in Figure 10(a) as an average of five experimental runs, and their relative standard deviations $\overline{RSD}_\rho$ are reported in Figure 12, after having performed the computations introduced in subsection 2.6.

The standard deviation shows that most of the variance in the powder density is created in the first tens of taps, possibly as a consequence of the cylinder filling procedure based on pouring. Nevertheless, the maximum $\overline{RSD}_\rho$ is 1.3% (blue bar in Figure 12) for PP-SLS-2, whereas its relative standard deviation $\sigma_{\overline{RSD}_\rho}$ is 0.1 (black error bar in Figure 12). This corresponds to an absolute $\overline{SD}_\rho$ of ± 0.007 g cm $^{-3}$ for PP-SLS-2. To provide some comparison with the ASTM B527 standard, which is the closest procedure to the methodology proposed in this paper that reported data on inter-laboratory repeatability, the standard deviation of an iron powder is shown in Table 4, and the results of the present work show improvement by a factor of 2.

4. Conclusion and outlook

In the current work, a novel methodology for the evaluation of flowability has been designed, tested and compared with the dynamic angle of repose and Hausner ratio. A commercially available tap density meter was upgraded with a camera that allowed to obtain the change of powder density in real-time. A representative sample of AM feedstock, including both metals and polymers, was chosen for this work through the analysis of four indicators (median diameter, elliptic smoothness, avalanche angle and Hausner ratio). The heterogeneity of the samples with respect to the proposed properties was confirmed and hence supports wide applicability of the proposed methodology in the field of AM. A novel indicator of compression flow is proposed, namely, the "normalized tapping modulus" $\tilde{T}_{15}$. It is calculated using a linear regression of the powder compaction over the first 15 taps. This quantity is unique to this test methodology, and correlations with size (D_{50V}) and shape (E_S) factors suggest that different compaction mechanisms exist for polymers and metals. For polymers, shape factors such as E_S play a significant role in the flowing behavior of the powder, whereas for metals only the effect of particle size could be shown with the data set at hand. When compared with the avalanche angle α_A, the fluidized flow measured by the dynamic angle of repose is a fair measure of the compressive flow pattern, at least for polymers. Metal samples, on the other hand, exhibit no statistically significant correlation between α_A and $\tilde{T}_{15}$, which implies that these different flow patterns induce a different response. The proposed methodology was evaluated through a repeatability study carried out on all ten powders by one operator, running five measurements for each powder, for a total of 50 measurements. The maximum relative standard deviation is 1.3%, and upon appropriate comparison with the repeatability study carried out by ASTM B527, the current methodology achieves better results in terms of within-operator repeatability, which can be quantified in a factor two of improvement. Outlook of the current study is to examine the usage of the settling time, defined as the time between the actual tap and the time at which the final V_{set}^i is reached, as indicator of powder flowability. Also, an even broader variety of metal powders characterized by different shape (e.g. water-atomized metal powders) and size (e.g. coarser powders for direct metal deposition) factors will be studied. Furthermore, correlation with in-process performances of each feedstock needs to be carried out. Considering the simplicity of implementing this measurement approach and because of widespread availability and low cost of tap density meters as quality assurance tools, the usage of a camera device has the potential to become a new standard methodology for the evaluation of powder flowability with regards to AM feedstock.

Figure 12 $\overline{RSD}_\rho$ for all materials, error bar showing the relative standard deviation $\sigma_{\overline{RSD}}$ among the five experimental trials

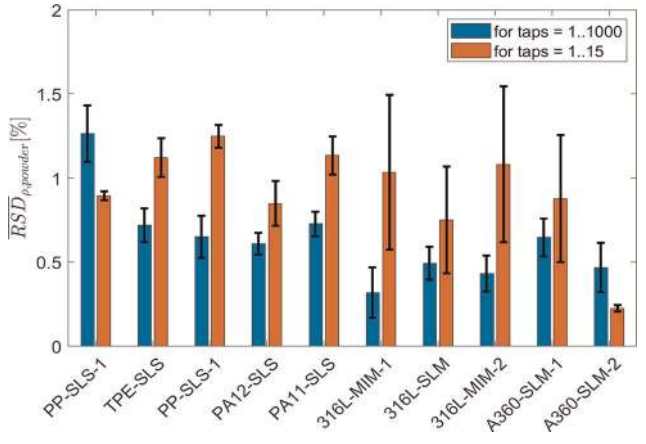

Table 3 $\tilde{T}_{15}$ for all materials

Material	$\tilde{T}_{15}$ (%)
316L-MIM-2	5.52
316 L-MIM-1	5.33
A360-SLM-1	4.68
PP-SLS-2	4.62
PA11-SLS	4.55
A360-SLM-2	4.43
PA12-SLS	4.30
316 L-SLM	3.78
PP-SLS-1	3.72
TPE-SLS	2.63

Table 4 $\overline{SD}_\rho$ comparison

Material	$\overline{SD}_\rho$	ρ_m	$\frac{\overline{SD}_\rho}{\rho_m}$
PP-SLS-2	0.007	1.000	0.007
Iron	0.100	7.874	0.013

References

Ali, U., Mahmoodkhani, Y., Shahabad, S.I., Esmaeilizadeh, R., Liravi, F., Sheydaeian, E., Huang, K.Y., Marzbanrad, E., Vlasea, M. and Toyserkani, E. (2018), "On the measurement of relative powder-bed compaction density in powder-bed additive manufacturing processes", *Materials &*

Design, Vol. 155, doi: 10.1016/j.matdes.2018.06.030, ISSN 02641275.

Amado, F. (2016), "Characterization and prediction of SLS processability of polymer powders with respect to powder flow and part warpage", PhD thesis, ETH Zürich.

ASTM International and ISO (2018), "ISO/ASTM 52900 – 18: additive manufacturing terminology".

ASTM International (2018), "ASTM B417 – 18: standard test method for apparent density of non-free-flowing metal powders using the carney funnel".

ASTM International (2015), "ASTM B527 – 15: standard test method for tap density of metal powders and compounds".

Baumann, F.-E. and Wilczok, N. (1998), "Preparation of precipitated polyamid powders of narrow particle size distribution and low porosity".

Berretta, S. (2015), "Poly ether ether ketone (PEEK) polymers for high temperature laser sintering (HT-LS)", p. 341.

Caffrey, T. and Wohler, T. (2019), *Wohlers Report 2019*, Technical report.

Gotoh, K., Masuda, H. and Higashitani, K. (2001), *Powder Technology Handbook, volume 10*, CRC Press, ISBN 9780429190186, doi: 10.1016/0921-5093(93)90508-c, available at: www.taylorfrancis.com/books/9781439831885

Haferkamp, L., Haudenschild, L., Spierings, A., Wegener, K., Riener, K., Ziegelmeier, S. and Leichtfried, G.J. (2021), "The influence of particle shape, powder flowability, and powder layer density on part density in laser powder bed fusion", *Metals*, Vol. 11 No. 3, doi: 10.3390/met11030418, ISSN 2075-4701.

Kleijnen, R., Schmid, M. and Wegener, K. (2019), "Production and processing of a spherical polybutylene terephthalate powder for laser sintering", *Applied Sciences*, Vol. 9 No. 7, p. 1308, doi: 10.3390/app9071308, ISSN 2076-3417, available at: www.mdpi.com/2076-3417/9/7/1308

Kiani, P., Scipioni Bertoli, U., Dupuy, A.D., Ma, K. and Schoenung, J.M. (2020), "A statistical analysis of powder flowability in metal additive manufacturing", *Advanced Engineering Materials*, Vol. 22 No. 10, doi: 10.1002/adem.202000022, ISSN 1438-1656.

Li, R., Shi, Y., Wang, Z., Li, W., Liu, J. and Jiang, W. (2010), "Densification behavior of gas and water atomized 316L stainless steel powder during selective laser melting", *Applied Surface Science*, Vol. 256 No. 13, ISSN 01694332, doi: 10.1016/j.apsusc.2010.02.030.

Ramanujan, S. (1914), "Modular equations and approximations to π", *Quarterly Journal of Mathematics*, Vol. 45, pp. 350-372.

Rietema, K. (1991), *The Dynamics of Fine Powders*, Elsevier Science Publishing Co., Inc., New York, NY, ISBN 1-85166-594-3.

Sames, W.J., List, F.A., Pannala, S., Dehoff, R.R. and Babu, S.S. (2016), "The metallurgy and processing science of metal additive manufacturing", *International Materials Reviews*, Vol. 61 No. 5, pp. 315-360, doi: 10.1080/09506608.2015.1116649, ISSN 0950-6608, available at: www.tandfonline.com/doi/full/10.1080/09506608.2015.1116649

Schmid, M., Amado, F. and Wegener, K. (2014), "Materials perspective of polymers for additive manufacturing with selective laser sintering", *Journal of Materials Research*, Vol. 29 No. 17, pp. 1824-1832, doi: 10.1557/jmr.2014.138, ISSN 0884-2914, available at: www.journals.cambridge.org/abstract_S0884291414001381

Schmid, M., Kleijnen, R., Vetterli, M. and Wegener, K. (2017), "Influence of the origin of polyamide 12 powder on the laser sintering process and laser sintered parts", *Applied Sciences*, Vol. 7 No. 5, p. 462, doi: 10.3390/app7050462, ISSN 2076-3417, available at: www.mdpi.com/2076-3417/7/5/462

Seyda, V. (2018), "Werkstoff- und prozessverhalten von metallpulvern in der laseradditiven fertigung", ISBN 978-3-662-58232-9.

Sillani, F., Kleijnen, R.G., Vetterli, M., Schmid, M. and Wegener, K. (2019), "Selective laser sintering and multi jet fusion: process-induced modification of the raw materials and analyses of parts performance", *Additive Manufacturing*, Vol. 27, pp. 32-41, doi: 10.1016/j.addma.2019.02.004, ISSN 22148604, available at: https://linkinghub.elsevier.com/retrieve/pii/S2214860418308972

Spierings, A.B., Voegtlin, M., Bauer, T. and Wegener, K. (2016), "Powder flowability characterisation methodology for powder-bed-based metal additive manufacturing", *Progress in Additive Manufacturing*, Vol. 1 Nos 1/2, doi: 10.1007/s40964-015-0001-4, ISSN 2363-9512.

Vetterli, M. (2019), "Powder optimization for laser sintering: an insight in powder intrinsic and extrinsic properties", PhD thesis, ETH Zurich.

Vock, S., Klöden, B., Kirchner, A., Weißgärber, T. and Kieback, B. (2019), "Powders for powder bed fusion: a review", *Progress in Additive Manufacturing*, Vol. 4 No. 4, doi: 10.1007/s40964-019-00078-6, ISSN 2363-9512, available at: http://link.springer.com/10.1007/s40964-019-00078-6

Ziegelmeier, S., Wollecke, F., Tuck, C., Goodridge, R. and Hague, R. (2013), "Characterizing the bulk & flow behaviour of LS polymer powders", *Solid Freeform Fabrication Symposium*, pp. 354-367.

Corresponding author

Francesco Sillani can be contacted at: sillani@inspire.ethz.ch